



# CHORUS

This is the accepted manuscript made available via CHORUS. The article has been published as:

## Effects of Surface Nonuniformities on the Mean Transverse Energy from Photocathodes

Siddharth Karkare and Ivan Bazarov

Phys. Rev. Applied **4**, 024015 — Published 24 August 2015

DOI: [10.1103/PhysRevApplied.4.024015](https://doi.org/10.1103/PhysRevApplied.4.024015)

# Effects of surface non-uniformities on the mean transverse energy from photocathodes

Siddharth Karkare\* and Ivan Bazarov

*CLASSE, Cornell University, Ithaca, New York, USA*

## Abstract

The performance of photoinjectors is limited by the lowest value of the mean transverse energy of the electrons obtained from photocathodes. The factors that influence the mean transverse energy are poorly understood. In this paper we develop models to calculate the effect of spatial work function variations and sub nanometer scale roughness and surface defects on the mean transverse energy. We show that these can limit the lowest value of MTE achieved and that atomically perfect surfaces will be required to further reduce the mean transverse energy obtained from photocathodes.

---

\* ssk226@cornell.edu

## I. INTRODUCTION

Photoinjectors provide electron beams for most 4<sup>th</sup> generation light sources like energy recovery linacs and free electron lasers and ultra-fast electron diffraction (UED) setups. For light source applications, the mean transverse energy (MTE) of electrons emitted from the photocathode limits the beam brightness obtained from photoinjectors[1]. For UED applications, the transverse coherence length of the electron beam is limited by the MTE obtained from photocathodes[2, 3]. The transverse coherence length sets the maximum size of the crystal unit cell for which a diffraction pattern can be resolved. Thus reducing the MTE from photocathodes can result in brighter electron beams and can allow UED of crystals with larger unit cells, for example, proteins.

Thermal emittance, which is the volume occupied by the electron beam in phase space, is a more familiar quantity to accelerator physicists. The normalized thermal emittance can be related to the MTE and the rms laser spot size on the cathode ( $\sigma_{l,x}$ ) through the relation  $\epsilon_{n,x} = \sigma_{l,x} \sqrt{\frac{\text{MTE}}{m_e c^2}}$  where  $m_e$  is the mass of an electron and  $c$  is the speed of light.

The theoretical lower limit to the MTE, given by a disorder induced scattering after emission, is 1-2 meV[4]. The smallest MTE demonstrated is in the 25-40 meV range from GaAs activated to negative electron affinity (NEA) using Cs and  $\text{NF}_3$ [5] under infrared illumination or from antimony films using near photoemission threshold wavelengths[6]. However, NEA-GaAs under infrared illumination has a very large response time in the 100 ps range[5] and antimony or other metals have very small quantum efficiency near photoemission threshold making them impractical for use in a photoinjector. In most photoinjectors, MTE in range of 100 meV to 1 eV is obtained from photocathodes[7]. Before reaching the theoretical limit, nearly two orders of magnitude improvement in MTE may be possible by engineering photocathode materials[8–10] that have smaller MTE with high quantum efficiencies and quick response times. However, no theory exists that can explain the observed MTE from photocathodes satisfactorily; several discrepancies exist.

One theory states that the MTE obtained from metal photocathodes is nearly one third the excess energy[11]. Here, the excess energy is defined as the energy difference between the incident photon and the work function of the material. An extension of this theory states that the MTE approaches the lattice temperature energy (25 meV at room temperature) as the excess energy tends to zero (near photoemission threshold)[12]. This theory produces

reasonable agreement with experimental data for metal and thin film alkali antimonide photocathodes[6, 13–15]. However, this theory does not take into account the effects of band structure, conservation of transverse momentum during emission and the effective mass of electrons in the lattice. In NEA-GaAs cathodes, the conservation of transverse momentum and small effective mass of electrons in the  $\Gamma$  valley should result in a MTE below 20 meV in infrared-green wavelengths[16, 17]. However, experimental results show a MTE of 25-120 meV in this wavelength range[5]. This discrepancy has been attributed to a surface scattering mechanism that redistributes the emitted electrons uniformly in the polar angle[16] or causes the  $\Gamma$  valley electrons near the surface to have an effective mass equal to the mass of a free electron[18]. However, no physical reason for this scattering mechanism has been identified.

To add to the complexity, the surfaces of frequently used photocathode materials are far from perfect. Photocathode surfaces often display roughness on the scales of 10s of nm[19–21]. Single crystal photocathodes which are atomically flat may exhibit surface reconstructions, atomic scale surface defects and monolayer adsorbates[22]. The effect of greater than 10 nm scale roughness on MTE has been studied[20, 21, 23, 24]. However, the effect of sub-nm scale surface defects, surface reconstructions and adsorbates on MTE remained unexplored.

Work function variations ranging from 1 meV to 100s of meV over less than nm scale to micron scale (along the cathode surface) can be caused due to atomic defects, atomic steps, surface reconstructions, localized charging, localized strains, grain boundaries and adsorbates[25–28]. The effect of such work function variations on MTE also remained unexplored.

In this paper, we investigate the effect of these work function variations and surface non-uniformities to show that it is important to consider their effects to achieve lower MTE. First we treat the effect of spatial work function variations on emitted electrons in a classical manner. The classical treatment is valid whenever the De Broglie wavelength of emitted electrons is much smaller than the scale of the spatial work function variation. Electric fields are formed in the vacuum region close to the cathode surface because of the work function variations. These electric fields deflect the emitted electrons and cause the MTE to increase. We estimate the rise in MTE due to these electric fields for a sinusoidal variation in the work function. We show that the effect of work function variation can be significant, but reduces

with increase in the kinetic energy of the emitted electron.

Next, we formulate a quantum mechanical emission model to include the effects of surface non-uniformities in the case when the De Broglie wavelength of the emitted electrons is similar to the scale of the surface non-uniformities. Such non-uniformities include atomic steps and defects, surface reconstructions, work function variations on a nm scale and adsorbates.

Finally, using the quantum mechanical formulation and the example of photoemission from activated GaAs photocathodes we show that sub nm scale roughness which can comprise of atomic steps, surface defects and surface reconstructions can limit the minimum MTE attainable. We also show that these can account for the surface scattering mechanisms responsible for increasing the theoretically predicted MTE from NEA-GaAs photocathodes

## II. CLASSICAL TREATMENT

Generally, electrons emitted from photocathodes have kinetic energies in the 10 meV to 1 eV range[7]. This results in a De Broglie wavelength of 1 nm to 10 nm. Thus spatial variations in work functions at a scale much greater than 10 nm can be treated in a classical manner. Work function variations at these large spatial scales can be caused due to localized surface charging, localized strains, patches of surface adsorbates and different grain orientations[25–28]. There have been previous attempts to study the effects of such patchy work function surfaces on low energy electron reflection[29], thermionic emission[30] and field emission[31].

The spatial variations in work function cause transverse (parallel to cathode surface) electric fields. These give a transverse kick to the emitted electrons and increase the MTE of the cathode. In this section, we calculate the electric fields formed due to a sinusoidal work function variation and estimate the effect they have on the MTE.

A similar effect, in which the transverse electric fields are caused due to the surface roughness of the cathode has been studied[23, 24, 32]. The calculation given below to estimate the effects of work function variation on MTE closely follows surface roughness effect calculation.

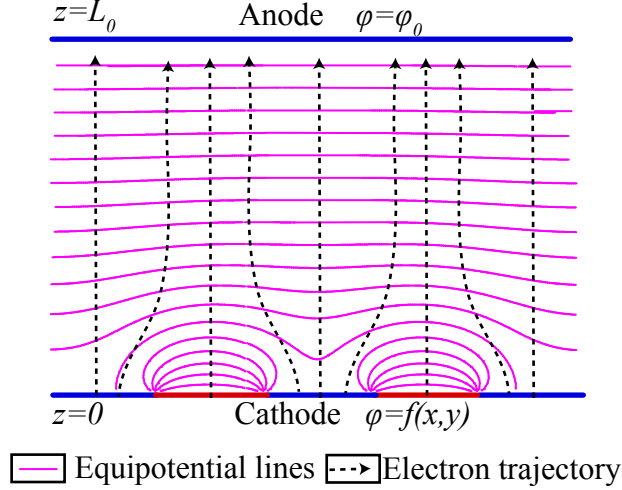


FIG. 1. Parallel plate capacitor model to calculate the effect of variation of work function on MTE. The equipotential lines get distorted near the cathode due to the non-uniform work function. This causes the electrons emitted from the cathode to gain transverse energy.

### A. Details of model and calculation

The potential of an electron right outside an electrode is the negative of bias applied to the electrode in volts plus the work function in eV. Thus variation in the work function essentially causes a variation in the surface potential of the electrode. In any photoinjector, a cathode is placed in a very high ( $\sim 1\text{-}50$  MV/m) longitudinal electric field. The variations in the surface potential cause the longitudinal electric field very close to the cathode surface to deform and acquire transverse components which decay rapidly as one goes away from the cathode. To model such a field we consider a parallel plate capacitor as shown in figure 1. It consists of a cathode that is grounded at  $z = 0$  and a parallel anode biased to a voltage  $\phi_0$  at  $z = L_0$ . Thus the longitudinal electric field at the cathode without the work function variation is  $E_0 = \phi_0/L_0$ . Let the work function variation on the cathode be given by  $f(x, y) \ll \phi_0$ . For simplicity we approximate the work function variation by a sinusoidal function,  $f(x, y) = h \sin\left(\frac{2\pi}{a}x\right) \sin\left(\frac{2\pi}{a}y\right)$ , where  $h$  is the amplitude of the work function variation and  $a$  is its spatial period.

Using the Laplace equation  $\nabla^2\phi = 0$  with boundary conditions  $\phi|_{z=0} = f(x, y)$  and

$\phi|_{z=L_0} = \phi_0$  we can obtain  $\phi$  in the region between the cathode and the anode as

$$\begin{aligned} \phi(x, y, z) = & \phi_0 \frac{z}{L_0} \\ & + h \frac{(e^{-z\gamma} - e^{(z-2L_0)\gamma})}{1 - e^{-2L_0\gamma}} \sin\left(\frac{2\pi}{a}x\right) \sin\left(\frac{2\pi}{a}y\right) \end{aligned} \quad (1)$$

where  $\gamma = \frac{2\sqrt{2}\pi}{a}$ . We also assume that  $a \ll L_0$  so that the transverse electric fields ( $E_x$  and  $E_y$ ) are nearly zero well before  $z = L_0$ . Using this approximation the potential can be given as

$$\begin{aligned} \phi(x, y, z) = & \phi_0 \frac{z}{L_0} \\ & + h e^{-z\gamma} \sin\left(\frac{2\pi}{a}x\right) \sin\left(\frac{2\pi}{a}y\right) \end{aligned} \quad (2)$$

From this the electric fields in the  $x, y$  and  $z$  can be calculated as:

$$\begin{aligned} E_x = & \frac{2\pi}{a} h e^{-z\gamma} \cos\left(\frac{2\pi}{a}x\right) \sin\left(\frac{2\pi}{a}y\right) \\ E_y = & \frac{2\pi}{a} h e^{-z\gamma} \sin\left(\frac{2\pi}{a}x\right) \cos\left(\frac{2\pi}{a}y\right) \\ E_z = & -E_0 + h\gamma e^{-z\gamma} \sin\left(\frac{2\pi}{a}x\right) \sin\left(\frac{2\pi}{a}y\right) \end{aligned} \quad (3)$$

The transverse velocities ( $v_x$  and  $v_y$ ) can be calculated by integrating the equations of motion. We integrate the equations of motion numerically using an 8-stage symplectic implicit integrator[33]. Electrons are launched from a fine grid of spacing  $a/40$  on the surface to obtain a fine sampling of all areas of the surface. The electrons are launched perpendicular to the surface with kinetic energy  $K$ . The initial transverse velocity and energy are set be zero. The electrons are tracked in the electric field given by equation 3 and the trajectories are calculated till the point the transverse electric fields become negligible and the transverse velocities are constant. The mean transverse energy is then calculated by averaging over the transverse energy of all the electrons. As the initial transverse velocities and energies are zero, this analysis gives us only the contribution of work function non-uniformities to the MTE.

An analytic expression for the MTE can also be obtained by making the assumption  $h/a \ll E_0$  and that the change in the  $x$  and  $y$  is negligible compared to  $a$ . With these

assumptions the expressions for the electric fields become:

$$\begin{aligned}
E_x &= \frac{2\pi}{a} h e^{-z\gamma} \cos\left(\frac{2\pi}{a} x_0\right) \sin\left(\frac{2\pi}{a} y_0\right) \\
E_y &= \frac{2\pi}{a} h e^{-z\gamma} \sin\left(\frac{2\pi}{a} x_0\right) \cos\left(\frac{2\pi}{a} y_0\right) \\
E_z &= -E_0
\end{aligned} \tag{4}$$

where  $x_0$  and  $y_0$  are the co-ordinates of the point from where the electron is launched.

Under these approximations the equations of motion can be integrated analytically to obtain the final transverse velocities,  $v_x$  and  $v_y$ . The MTE can be calculated by averaging the transverse kinetic energy over the entire surface as  $\text{MTE} = \frac{1}{2} m_e \frac{\int \int (v_x^2 + v_y^2) dx dy}{\int \int dx dy}$ . The MTE thus obtained can be given by the analytic expression:

$$\text{MTE} = \frac{\pi^2 h^2 e}{4\sqrt{2} a E_0} e^{-\frac{\beta^2}{2\alpha}} \text{erfc}^2\left(\frac{\beta}{2\sqrt{\alpha}}\right) \tag{5}$$

where  $\alpha = \frac{\sqrt{2}\pi e E_0}{a m_e}$  and  $\beta = \frac{4\pi\sqrt{K}}{a\sqrt{m_e}}$ .

## B. Results

Figure 2 shows the MTE calculated by numerically tracking electron trajectories for initial kinetic energies ( $K$ ) of 20 meV and 60 meV and  $a = 100$  nm. Figure 2a shows the MTE calculated at zero electric field as a function of  $h$  for  $K = 20$  meV. We can see that values of  $h$  as low as 0.1 V can result in MTE higher than 20 meV.

Figure 2b shows the variation of MTE with electric field for two cases:  $h = 0.1$  V and  $K = 20$  meV;  $h = 0.6$  V and  $K = 60$  meV. We can see that for both cases the MTE is nearly constant with electric field ( $E_0$ ) so long as the electric field is below  $h/a$  (shown by the black lines in the figure). If  $E_0 < h/a$ , the first term in the expression for  $E_z$  in equation 3 can be ignored, making the electric field near the cathode surface independent of  $E_0$ . Hence the MTE does not vary much with  $E_0$  in this regime. However, as the electric field rises beyond  $h/a$ , the electrons are extracted away from the cathode surface more quickly. This gives them less time to interact with the transverse electric fields close to the surface and hence the MTE reduces. This reduction in MTE with electric field should be easily observable in with electric fields in the range of 1-10 MV/m if the MTE is indeed limited by work function non-uniformities on a classical scale. Such a change with electric field is contrary



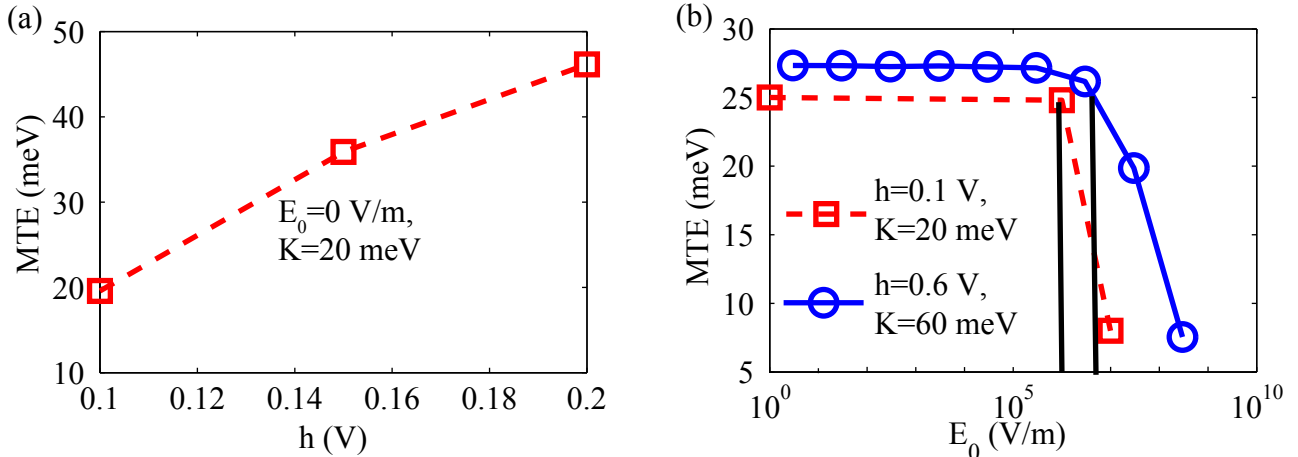


FIG. 2. (a) Variation of MTE with  $h$ . The external electric field was set to zero for these calculations. (b) Variation of the MTE with the electric field,  $E_0$ . The value of  $a$  was set to 100 nm for these calculations.  $h/a$  for the red curve is 1 MV/m and for the blue curve is 6 MV/m (shown by the black lines). The MTE is nearly independent of the electric field when  $E_0 < h/a$ , beyond that it reduces sharply with the electric field.

to the change expected due to the 10-100 nm scale surface roughness[23, 24]. Due to the surface roughness effect, the MTE increases with increasing electric field.

MTE also reduces with increase in initial kinetic energy ( $K$ ) and increase in the period  $a$ . Figure 3 a and b show the variation of MTE with initial kinetic energy and the period  $a$  respectively, for  $h = 0.1$  V and  $E_0 = 10$  MV/m. These parameters are such that the approximations made to estimate the MTE in equation 5 are valid. The MTE in figure 3 is calculated from this equation.

In short, we see that work function variations of  $\sim 0.1$  eV over a scale of  $\sim 100$  nm can limit the MTE to 20-30 meV if the kinetic energy of electrons emitted electrons is near 20 meV. This is often the case with near threshold photoemission, where the excess energy and hence the kinetic energy of emitted electrons is  $\sim 25$  meV (thermal energy at room temperature). Work function variations of similar magnitudes have been experimentally observed on various surfaces due to localized surface charging, localized strains, patches of surface adsorbates and different grain orientations[25–28]. Hence, in order to obtain MTE of less than 20 meV it will be necessary to ensure the spatial uniformity of cathode work functions. It is also important to measure the work function variations on practical cathode

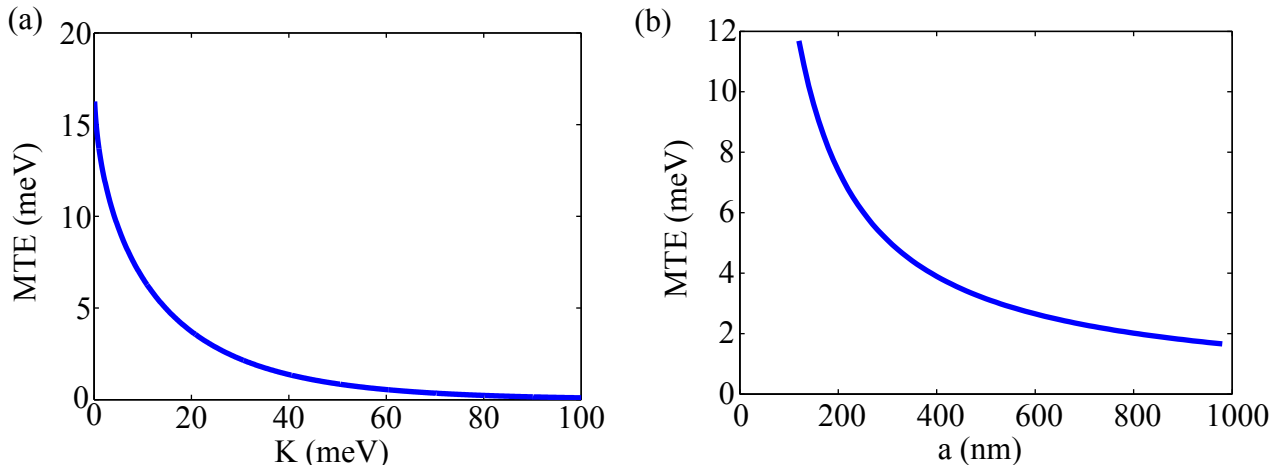


FIG. 3. (a) Variation of MTE with the initial kinetic energy.  $E_0 = 10$  MV/m,  $h = 0.1$  V and  $a = 100$  nm (b) Variation of MTE with the the period  $a$ .  $E_0 = 10$  MV/m,  $h = 0.1$  V and  $K = 1$  meV.

surfaces.

### III. QUANTUM TREATMENT

In this section, we develop an emission model that takes into account surface non-uniformities of spatial scales less than or comparable to the De Broglie wavelength of the emitted electrons and show how conservation of transverse momentum can be violated in their presence.

#### A. Emission model

The emission model described here assumes a semiconductor cathode, however it can easily be extended to metallic cathodes.

The model assumes Spicer's 3-step process of photoemission[34]. The first two steps of electron excitation from valence band to conduction band and subsequent electron transport to the surface in the conduction band are well understood[16]. Here we discuss the last step of emission to include the effects of surface non-uniformities.

Figure 4a shows the potential used to describe the cathode-vacuum interface. The electrons approach the surface in the form of plane waves with crystal momentum  $\mathbf{k}_{\text{in}}$  and energy

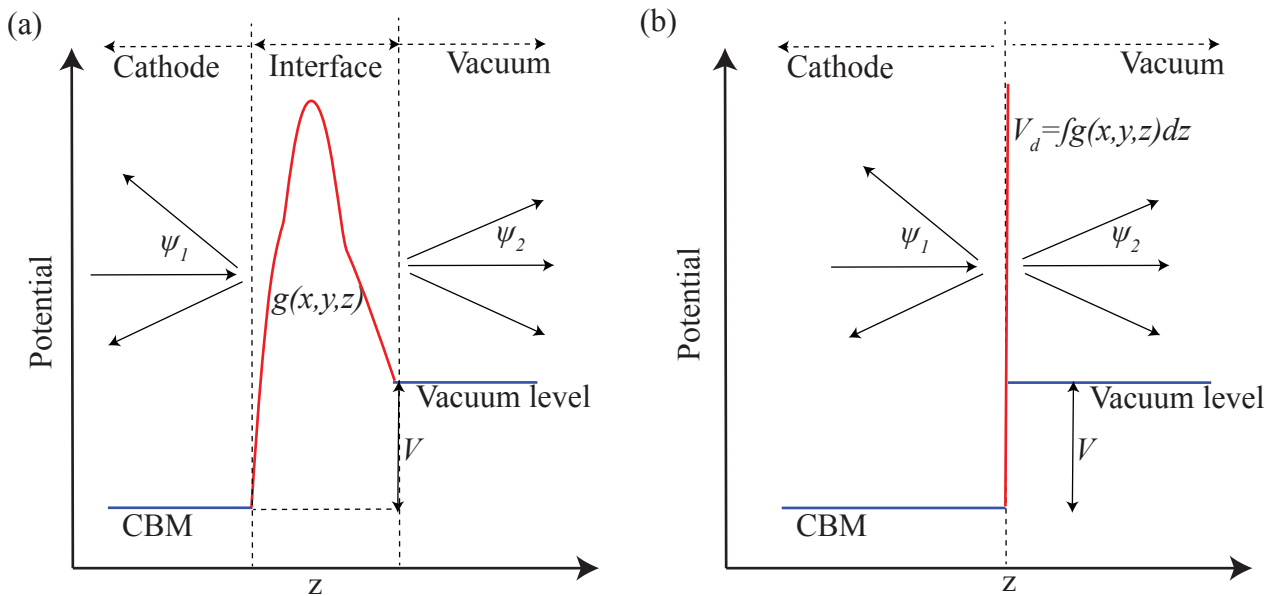


FIG. 4. (a) Potential to model the surface non-uniformities along with the incoming and scattered wave functions (b)  $\delta$  function approximation to the potential used to account for surface non-uniformities

$E_c$ . We assume that the energy and the crystal momentum are related via the parabolic, spherical dispersion relation

$$E_c = \frac{\hbar^2 |\mathbf{k}_{\text{in}}|^2}{2m^*} \quad (6)$$

where  $m^*$  is the effective mass of the electron inside the cathode. The potential within the cathode and in vacuum is assumed to be constant. The interface is represented by a potential  $g(x, y, z)$  along with a step of height  $V$ . The potential  $g(x, y, z)$  includes all interface effects, transverse variations of the potential due to surface non-uniformities and defects and electric fields due to work function variations.  $g(x, y, z)$  is zero in the cathode bulk and in vacuum, but is non-zero in the interface region. The incoming electron wave gets scattered due to the potential  $g(x, y, z)$ . Part of the incoming wave gets reflected and the rest gets transmitted into vacuum. In this study, we assume a field free region in the vacuum. This approximation is true for small electric fields generally found in DC guns.

We approximate the wave function of the incoming electron with a plane wave  $\psi_{in} = e^{i(\mathbf{k}_{\text{inr}}\mathbf{r} + k_{1inz}z)}$  where  $\mathbf{k}_{\text{inr}} = k_{inx}\vec{\mathbf{x}} + k_{iny}\vec{\mathbf{y}}$  is the transverse component and  $k_{1inz}\vec{\mathbf{z}}$  is the longitudinal component of the wave vector  $\mathbf{k}_{\text{in}}$  and  $\mathbf{r}$  is the position vector in the transverse

direction.

The challenge is to calculate the scattering of the incoming plane wave due to the interface potential  $g(x, y, z)$ . A similar problem has been studied extensively to model electron transport across semiconductor heterojunctions[35–40]. The most general solution to this problem is obtained by solving the Lippmann-Schwinger equation[35, 41]. Solutions using tight-binding like approach[36–38] and transfer matrix approach have also been attempted[39].

Here, we simplify this problem by replacing the interface potential  $g(x, y, z)$  by a  $\delta$  function whose height varies in  $x$  and  $y$  and is given by  $V_d(x, y) = \int g(x, y, z) dz$ . Such a simplification is valid when the interface region is much smaller than the wavelength of the emitted electrons. Figure 4b shows the potential with this  $\delta$  function approximation. The Hamiltonian for this system can be written as

$$H = -\frac{\hbar^2}{2} \nabla \left( \frac{1}{m} \nabla \right) + V \cdot S(z) + V_d(x, y) \delta(z) \quad (7)$$

where  $m = m^*$  if  $z < 0$  and  $m = m_e$  if  $z \geq 0$  and  $S(z)$  is the heavy side function.

$V_d(x, y)$  can be expanded in terms of its Fourier components as

$$V_d(x, y) = \sum_{\eta} V_{\mathbf{k}_{r\eta}} e^{i(\mathbf{k}_{r\eta} \cdot \mathbf{r})} \quad (8)$$

The wave function of the incoming and the reflected electrons within the photocathode can then be written as

$$\begin{aligned} \psi_1 = \psi_{in} + \alpha_{\mathbf{k}_{inr}} e^{i(\mathbf{k}_{inr} \cdot \mathbf{r} - k_{1in} z)} + \\ \sum_{\eta} e^{i(\mathbf{k}_{r\eta} \cdot \mathbf{r} - k_{1z\eta} z)} \end{aligned} \quad (9)$$

where  $\mathbf{k}_{r\eta}$  and  $k_{1z\eta} \vec{z}$  are the transverse and longitudinal components, respectively, of the wave vectors into which the incoming electron wave is scattered due to reflection from the barrier  $V_d$  and  $\alpha_{\mathbf{k}_{r\eta}}$  are the probability coefficients for the respective scattered wave vectors.

The wave function of the electrons transmitted into vacuum can be written as

$$\psi_2 = (1 + \alpha_{\mathbf{k}_{inr}}) e^{i(\mathbf{k}_{inr} \cdot \mathbf{r} + k_{2in} z)} + \sum_{\eta} \alpha_{\mathbf{k}_{r\eta}} e^{i(\mathbf{k}_{r\eta} \cdot \mathbf{r} + k_{2z\eta} z)} \quad (10)$$

where  $\mathbf{k}_{r\eta}$  and  $k_{2z\eta} \vec{z}$  are the transverse and longitudinal components, respectively, of the wave vectors into which the incoming electron wave is scattered in vacuum.

$\psi_1$  and  $\psi_2$  are general and satisfy the condition  $\psi_1 = \psi_2$  at  $z = 0$ .

We assume that this scattering is elastic in nature. Hence from the conservation of energy, all the reflected wave vectors satisfy the relation

$$\frac{\hbar^2 (k_{r\eta}^2 + k_{1z\eta}^2)}{2m^*} = E_c \quad (11)$$

and all the transmitted wave vectors satisfy the relation

$$\frac{\hbar^2 (k_{r\eta}^2 + k_{2z\eta}^2)}{2m_e} = E_v = E_c - V \quad (12)$$

$$\frac{\hbar^2 (k_{inr}^2 + k_{2inz}^2)}{2m_e} = E_v = E_c - V \quad (13)$$

where  $E_v$  is the kinetic energy of the electron emitted into vacuum.

Now the coefficients  $\alpha_{\mathbf{k}_{inr}}$  and  $\alpha_{\mathbf{k}_{r\eta}}$  can be calculated by integrating the Schrodinger equation for the Hamiltonian given in equation 7 across the  $\delta$  barrier in the  $z$  direction from  $0^-$  to  $0^+$  and comparing the coefficients of the same exponents as done by Liu and Coon[40].

For a 1-D sinusoidal  $\delta$  barrier at the surface, given by  $V_d = 2V_0 \cos(k_s x)$  the set of equations to calculate  $\alpha$  coefficients can be written in the form of a tridiagonal matrix system as

$$A \begin{pmatrix} \vdots \\ \alpha_{k_{inx}-k_s} \\ \alpha_{k_{inx}} \\ \alpha_{k_{inx}+k_s} \\ \vdots \end{pmatrix} = \begin{pmatrix} \vdots \\ 0 \\ V_0 \\ R(k_{inx}) \\ V_0 \\ 0 \\ \vdots \end{pmatrix}, \quad (14)$$

$$A = \begin{pmatrix} \ddots & \vdots & \vdots & \vdots & \cdots \\ \cdots & D(k_{inx} - k_s) & -V_0 & 0 & \cdots \\ \cdots & -V_0 & D(k_{inx}) & -V_0 & \cdots \\ \cdots & 0 & -V_0 & D(k_{inx} + k_s) & \cdots \\ \cdots & \vdots & \vdots & \vdots & \ddots \end{pmatrix}$$

where,  $R(k_x) = \frac{i\hbar^2}{2} \left( \frac{k_{2z}}{m_e} - \frac{k_{1z}}{m^*} \right)$  and  $D(k_x) = \frac{\hbar^2}{2i} \left( \frac{k_{2z}}{m_e} + \frac{k_{1z}}{m^*} \right)$ .  $k_{1z}$  and  $k_{2z}$  can be calculated in terms of  $k_r$  from equations 11 and 12.

By solving this system one can obtain the coefficients  $\alpha$  in terms of the transverse wave vector of the incoming plane wave  $k_{inx}$  and the  $\delta$  barrier at the interface. The probability of transmission into one of the scattered components with transverse wave vector  $k_x \neq k_{inx}$  is given by[39]

$$T_{k_x} = \frac{m^* |\alpha_{k_x}|^2 (k_{2z} + k'_{2z})}{2m_e k_{1z}} \quad (15)$$

and the probability of unscattered transmission is given by

$$T_{k_{inx}} = \frac{m^* |1 + \alpha_{k_{inx}}|^2 (k_{2inz} + k'_{2inz})}{2m_e k_{1inz}} \quad (16)$$

The MTE due to the emission of the plane wave can then be given by

$$\text{MTE} = \frac{\sum_m \frac{\hbar^2 (k_{inx} + mk_s)^2 T_{k_{inx} + mk_s}}{2m_e}}{\sum_m T_{k_{inx} + mk_s}} \quad (17)$$

## B. Example of NEA-GaAs

NEA-GaAs cathodes should exhibit MTE of less than 10 meV in infrared light due to the small effective mass of  $\Gamma$  valley electrons and the conservation of transverse momentum during emission[16]. However, the smallest MTE measured from these cathodes is in the 25-40 meV range[5, 8, 42].

Using the emission model discussed in section IIIA, we show that surface non-uniformities including atomic surface defects and surface reconstructions could explain the large MTE observed from GaAs.

In our model of the activated GaAs surface, we assume that the work function is uniform, and the barrier due at the interface is negligible. The surface is modeled only by a step rise in the potential along with a sudden change in effective mass as shown in figure 5a. For the activated GaAs (100) surface, the conduction band minimum (CBM) at the surface is  $\sim 0.5$  V below the vacuum level[16], making the height of the step barrier  $V = 0.5$  V. In our model we assume that the band bending is very gradual and hence ignore any slope to the CBM near the surface. This assumption is true for very lightly doped GaAs cathodes or for layered GaAs cathodes with un-doped top layer[8].

The atomic defects, steps and reconstructions of the surface are modeled by introducing a sinusoidal surface ‘roughness’ in the  $x$  direction. The  $z$  position of the potential step at the interface changes due to this roughness and is given by  $z = t \cos\left(\frac{2\pi}{\lambda}x\right)$ , where  $t = 1$

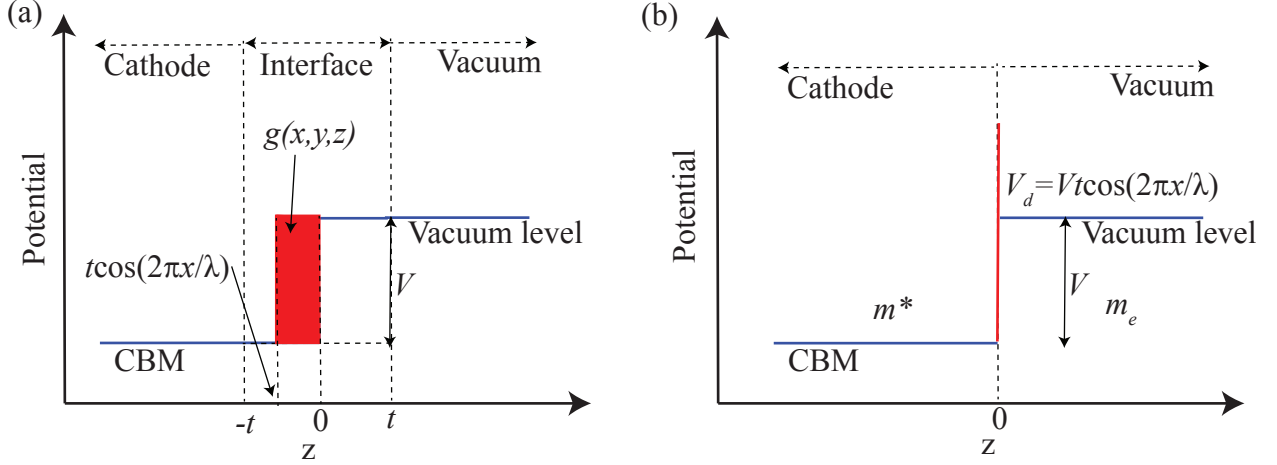


FIG. 5. (a) Potential to model the GaAs surface. The non-uniformities are modeled using a small sinusoidal roughness of in the  $x$  direction (b) The sinusoidal roughness is approximated using a  $\delta$  function.

nm, making the rms roughness only 0.7 nm.  $\lambda$  is the periodicity of the surface roughness. As shown in figure 5b, this roughness can be approximated by a  $\delta$  function barrier whose height is given by  $Vt \cos\left(\frac{2\pi}{\lambda}x\right) = 0.5 \cos\left(\frac{2\pi}{\lambda}x\right)$  nm-V. For this approximation to be valid the wavelength of the electrons must be much larger than 1 nm. The MTE can be estimated from equation 17.

Figure 6a shows MTE as a function of the period of the surface roughness ( $\lambda$ ) for various kinetic energies of emitted electrons. The transverse momentum of the incoming electrons was set to zero. Thus the MTE calculated is purely due to the effect of sub-nm scale roughness. We can see that the MTE can increase with increasing kinetic energy of the electrons.

A realistic distribution of the electron wave-vectors emitted from the surface was calculated from the Monte Carlo based electron transport simulation[16] for incident photon energy of 1.6 eV. The MTE from such a distribution was calculated using equation 17 with  $t = 1$  nm. Figure 6b shows this MTE for various values of  $\lambda$ . The MTE obtained experimentally and from the Monte Carlo simulation without assuming any surface scattering are also shown.

Scattering occurs only when the electron wavelength is comparable to the period of the surface non-uniformities. Hence, the MTE calculated using the quantum model for surface

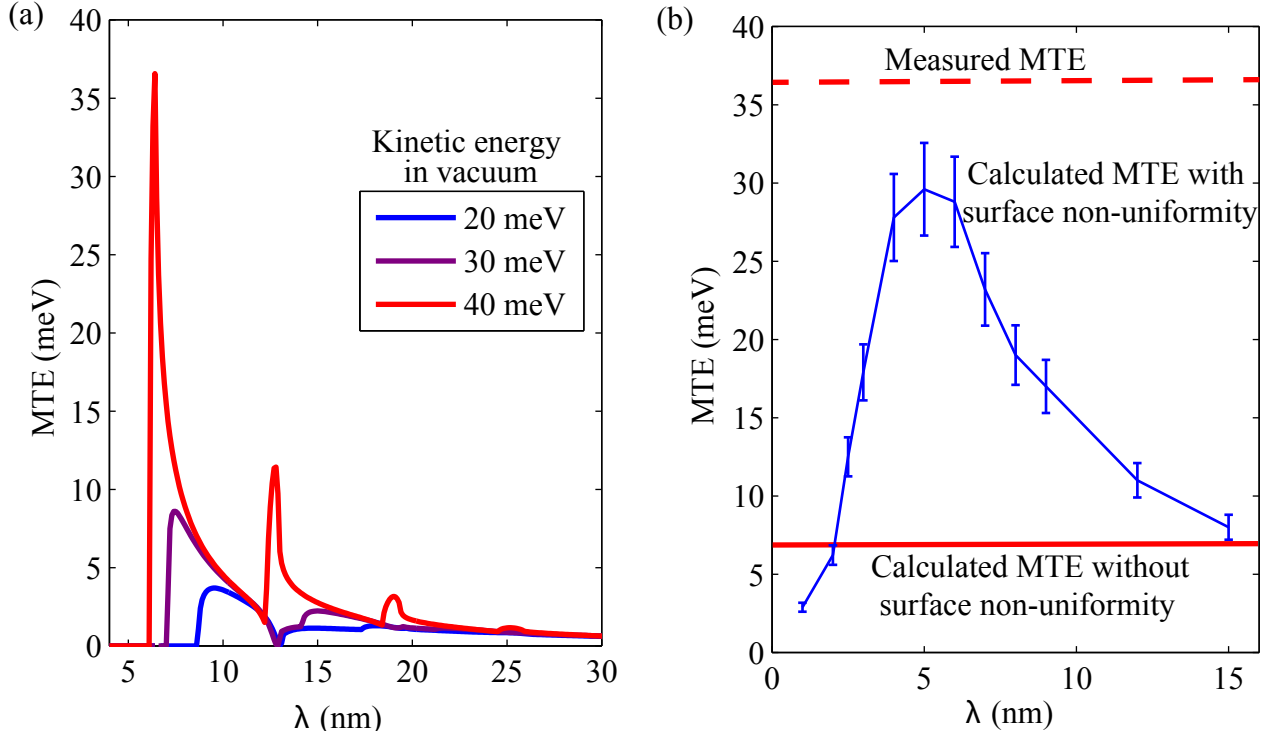


FIG. 6. (a) Calculated MTE as a function of the period ( $\lambda$ ) of the surface non-uniformity for various electron energies. A spike in MTE occurs whenever the electron energy is sufficient to allow scattering into a higher order transverse wave-vector. (b) Calculated MTE as a function of the period ( $\lambda$ ) for a realistic distribution of incoming wave-vectors. The MTE measured experimentally and calculated without the surface non-uniformity are also shown.

non-uniformities initially rises with increasing  $\lambda$  and then decreases. The MTE is comparable to the measured value if the period of non-uniformities is 4-6 nm. Thus it is possible to explain the higher MTE measured from GaAs cathodes.

Although we discuss a specific case of GaAs cathodes, a similar argument can be made for any cathode material. Hence, to obtain very low MTE it may be necessary to make the surface devoid of sub-nm scale roughness and essentially have a atomically perfect surface.

As the excess energy of the photons increases, electrons emitted have a higher kinetic energy and a smaller wavelength. For kinetic energy equal to 0.2 eV, the De Broglie wavelength becomes lower than 3 nm, questioning the  $\delta$  function approximation. More general solutions to the scattering problem should be implemented to investigate this regime.



## IV. CONCLUSION

We investigated the effect of surface non-uniformities on the MTE of photocathodes.

First, we developed a classical model to estimate the effect of the work function variations on the MTE of emitted electrons. Using this model, we conclude that the surface work function variations as low as 0.1-0.2 eV can at length scales of  $\sim 100$  nm can be sufficient to limit the MTE of emitted electrons to 20-30 meV (very close to the minimum measured value of 25 meV).

Second, we developed a quantum mechanical model to study the effects of surface uniformities of transverse spatial extent comparable to the wavelength of the emitted electrons. Using this model we show that sub-nm scale surface roughness, atomic scale surface defects and surface reconstructions have can affect the MTE significantly. Using NEA-GaAs cathodes as an example we show how such sub-nm scale defects could limit the minimum measured MTE and account for various surface scattering effects.

Both of these effects have been ignored in photoemission models developed so far. The calculations presented here show that a detailed study of both these effects should be performed and included in photoemission models in order to explain photoemission accurately.

The detail study of work function variations on  $\mu\text{m}$  to nm scales, sub-nm scale surface roughness and surface structures is missing. These surface properties can change once the cathode samples are exposed to air. Hence an in-situ measurement of such surface characteristics of real photocathode surfaces is required to obtain accurate results. The calculations presented in this study show that the MTE from photocathodes may be limited by these effects underscoring the importance of measuring these properties.

## V. ACKNOWLEDGMENTS

The authors would like to thank Laurent Boulet for his help with the classical part of the calculations and Dr. Dimitre Dimitrov for his helpful suggestions regarding the paper.

This work was supported by the Department of Energy under grant number DE-

- 
- [1] I. V. Bazarov, B. M. Dunham, and C. K. Sinclair, “Maximum achievable beam brightness from photoinjectors,” *Phys. Rev. Lett.* **102**, 104801 (2009).
- [2] P. Musumeci, J. T. Moody, C. M. Scoby, M. S. Gutierrez, H. A. Bender, and N. S. Wilcox, “High quality single shot diffraction patterns using ultrashort megaelectron volt electron beams from a radio frequency photoinjector,” *Rev. Sci. Instr.* **81**, 013306 (2010).
- [3] T. van Oudheusden, E. F. de Jong, S. B. van der Geer, W. P. E. M. Op t Root, O. J. Luiten, and B. J. Siwick, “Electron source concept for single-shot sub-100 fs electron diffraction in the 100 keV range,” *J. Appl. Phys.* **102**, 093501 (2007).
- [4] J. M. Maxson, I. V. Bazarov, W. Wan, H. A. Padmore, and C. E. Coleman-Smith, “Fundamental photoemission brightness limit from disorder induced heating,” *New J. Phys.* **15**, 103024 (2013).
- [5] I. V. Bazarov, B. M. Dunham, Y. Li, X. Liu, D. G. Ouzounov, C. K. Sinclair, F. Hannon, and T. Miyajima, “Thermal emittance and response time measurements of negative electron affinity photocathodes,” *J. Appl. Phys.* **103**, 054901 (2008).
- [6] J. Feng, J. Nasiatka, W. Wan, T. Vecchione, and H. A. Padmore, “A novel system for measurement of the transverse electron momentum distribution from photocathodes,” *Rev. Sci. Instrum.* **86**, 015103 (2015).
- [7] D. H. Dowell, I. Bazarov, B. Dunham, K. Harkay, C. Hernandez-Garcia, R. Legg, H. Padmore, T. Rao, J. Smedley, and W. Wan, “Cathode r&d for future light sources,” *Nucl. Instrum. Methods Phys. Res. A* **622**, 685 (2010).
- [8] S. Karkare, L. Boulet, L. Cultrera, B. Dunham, X. Liu, W. Schaff, and I. Bazarov, “Ultra-bright and ultrafast iiv semiconductor photocathodes,” *Phys. Rev. Lett* **112**, 097601 (2014).
- [9] T. C. Droubay, S. A. Chambers, A. G. Joly, W. P. Hess, K. Nemeth, K. C. Harkay, and L. Spentzouris, “Metal-insulator photocathode heterojunction for directed electron emission,” *Phys. Rev. Lett.* **112**, 067601 (2014).
- [10] K. Nemeth, K. C. Harkay, M. van Veenendaal, L. Spentzouris, M. White, K. Attenkofer, and G. Srajer, “High-brightness photocathodes through ultrathin surface layers on metals,” *Phys. Rev. Lett.* **104**, 046801 (2010).

- [11] D.H. Dowell and J.F. Schmerge, “Quantum efficiency and thermal emittance of metal photocathodes,” *Phys. Rev. ST Accel. Beams* **12**, 074201 (2009).
- [12] T. Vecchione, D. Dowell, W. Wan, J. Feng, and H. A. Padmore, “Quantum efficiency and transverse momentum from metals,” in *Proceedings of FEL, New York* (2013).
- [13] L. Cultrera, I. Bazarov, A. Bartnik, B. Dunham, S. Karkare, R. Merluzzi, and M. Nichols, “Thermal emittance and response time of a cesium antimonide photocathode,” *Appl. Phys. Lett.* **99**, 152110 (2011).
- [14] I. Bazarov, L. Cultrera, A. Bartnik, B. Dunham, S. Karkare, Y. Li, X. Liu, J. Maxson, and W. Roussel, “Thermal emittance measurements of a cesium potassium antimonide photocathode,” *Appl. Phys. Lett.* **98**, 224101 (2011).
- [15] L. Cultrera, S. Karkare, H. Lee, X. Liu, I. Bazarov, and B. Dunham, “Cold electron beams from cryo-cooled, alkali antimonide photocathodes,” arXiv **1504.05920** (2015).
- [16] S. Karkare, D. Dimitrov, W. Schaff, L. Cultrera, A. Bartnik, X. Liu, E. Sawyer, T. Esposito, and I. Bazarov, “Monte carlo charge transport and photoemission from negative electron affinity gaas photocathodes,” *J. Appl. Phys.* **113**, 104904 (2013).
- [17] R. L. Bell, *Negative affinity electron devices* (Clarendon press, Oxford).
- [18] G. Vergara, A. Herrera-Gomez, and W. E. Spicer, “Electron transverse energy distribution in gaas negative electron affinity cathodes: Calculations compared to experiments,” .
- [19] S. Schubert, M. Ruiz-Oses, I. Ben-Zvi, T. Kamps, X. Liang, E. Muller, K. Muller, H. Padmore, T. Rao, X. Tong, T. Vecchione, and J. Smedley, “Bi-alkali antimonide photocathodes for high brightness accelerators,” *APL Materials* **1**, 032119 (2013).
- [20] H. J. Qian, C. Li, Y. C. Du, L. X. Yan, J. F. Hua, W. H. Huang, and C. X. Tang, “Experimental investigation of thermal emittance components of copper photocathode,” *Phys. Rev. ST Accel. Beams* **15**, 040102 (2012).
- [21] S. Karkare and I. Bazarov, “Effect of nanoscale surface roughness on transverse energy spread from gaas photocathodes,” *Appl. Phys. Lett.* **98**, 094104 (2011).
- [22] S. Karkare, L. Boulet, A. Singh, R. Hennig, and I. Bazarov, “Ab initio studies of cs on gaas (100) and (110) surfaces,” *Phys. Rev. B* **91**, 035408 (2015).
- [23] S. Karkare, I. Bazarov, L. Cultrera, A. Iyer, X. Liu, and W. Schaff, “Effect of surface roughness on the emittance from gaas photocathode,” in *Proceedings of Particle Accelerator Conference, New York, NY, USA* (2011).

- [24] D. J. Bradley, M. B. Allenson, and B. R. Holeman, “The transverse energy of electrons emitted from gaas photocathodes,” .
- [25] Th. Glatzel, S. Sadewasser, R. Shikler, Y. Rosenwaks, and M. Ch. Lux-Steiner, “Kelvin probe force microscopy on iiii semiconductors: the effect of surface defects on the local work function,” .
- [26] W. Melitz, J. Shen, A. Kummel, and S. Lee, “Kelvin probe force microscopy and its application,” *Surf. Sci. Rep.* **66**, 1 (2011).
- [27] C. Barth and C. R. Henry, “Kelvin probe force microscopy on surfaces of uhv cleaved ionic crystals,” *Nanotechnology* **17**, S155 (2006).
- [28] Nicolas Gaillard, Denis Mariolle, Francois Bertin, Mickael Gros-Jean, and Ahmad Bsiesy, “Metal electrodes work function measurement at deca-nanometer scale using kelvin probe force microscope: a step forward to the comprehension of deposition techniques impact on devices electrical properties,” in *Symposium E Gate Stack Scaling Materials Selection, Role of Interfaces, and Reliability Implications*, MRS Proceedings, Vol. 917 (2006).
- [29] H. Heil, “Electron reflection coefficient at zero energy. ii. computer experiments on the reflection of slow electrons in the electrostatic field of surface patches,” *Phys. Rev.* **164**, 887 (1967).
- [30] E. A. Adler and R. T. Longo, “Effect of nonuniform work function on space-charge-limited current,” *J. Appl. Phys.* **59**, 1022 (1986).
- [31] J. Robertson, “Mechanisms of electron field emission from diamond, diamond-like carbon, and nanostructured carbon,” *J. Vac. Sci. Technol. B* **17**, 659 (1999).
- [32] Zhe Zhang and Chuanxiang Tang, “Analytical study on emittance growth caused by roughness of a metallic photocathode,” *Phys. Rev. ST Accel. Beams* **18**, 053401 (2015).
- [33] E. Harier, C. Lubich, and G. Wanner, *Geometric Numerical Integration - Structure Preserving Algorithms for Ordinary Differential Equations* (Springer Series in Computational Mathematics, 2006).
- [34] W. E. Spicer, “Negative affinity 35 photocathodes: Their physics and technology,” *Appl. Phys. A* **12**, 115 (1977).
- [35] Peter Johansson, “Theory of interface-roughness scattering in resonant tunneling,” *Phys. Rev. B* **48**, 8938 (1993).
- [36] D. Z.-Y. Ting, E. T. Yu, and T. C. McGill, “Multiband treatment of quantum transport in

- interband tunnel devices,” *Phys. Rev. B* **45**, 3583 (1992).
- [37] D. Z. Y. Ting, S. K. Kirby, and T. C. McGill, “Interface roughness effects in resonant tunneling structures,” *Appl. Phys. Lett.* **64**, 2004 (1994).
- [38] D. Z. Y. Ting, S. K. Kirby, and T. C. McGill, “Three dimensional simulations of quantum transport in semiconductor nanostructures,” *J. Vac. Sci. Technol. B* **11**, 1738 (1993).
- [39] W. T. Dietze and R. B. Darling, “Coherent electron transport across semiconductor heterojunctions with rough interfaces,” *Phys. Rev. B* **53**, 3925 (1996).
- [40] H. C. Liu and D. D. Coon, “Interface roughness and island effects on tunneling in quantum wells,” *J. Appl. Phys.* **64**, 6785 (1988).
- [41] Kai Sandfort, *The Factorization Method for Inverse Scattering from Periodic Inhomogeneous Media*, Ph.D. thesis, Karlsruhe Institut für Technologie (2010).
- [42] S. Karkare, L. Cultrera, Y. Hwang, R. Merluzzi, and I. Bazarov, “2-d energy analyzer for low energy electrons,” *Rev. Sci. Instrum.* **86**, 033301 (2015).